




# Chronic mild stress alters synaptic plasticity in the nucleus accumbens through GSK3 $\beta$ -dependent modulation of Kv4.2 channels

Giuseppe Aceto<sup>a</sup>, Claudia Colussi<sup>b</sup>, Lucia Leone<sup>a,c</sup>, Salvatore Fusco<sup>a,c</sup>, Marco Rinaudo<sup>a</sup>, Federico Scala<sup>d</sup>, Thomas A. Green<sup>e</sup>, Fernanda Laezza<sup>e</sup>, Marcello D'Ascenzo<sup>a,c,1,2</sup> , and Claudio Grassi<sup>a,c,2</sup>

<sup>a</sup>Department of Neuroscience, Università Cattolica del Sacro Cuore, 00168 Rome, Italy; <sup>b</sup>Istituto di Analisi dei Sistemi ed Informatica "Antonio Ruberti," National Research Council, 00185 Rome, Italy; <sup>c</sup>Fondazione Policlinico Universitario A. Gemelli, Istituto di Ricovero e Cura a Carattere Scientifico (IRCCS), 00168 Rome, Italy; <sup>d</sup>Department of Neuroscience, Baylor College of Medicine, Houston, TX 77030; and <sup>e</sup>Department of Pharmacology and Toxicology, University of Texas Medical Branch, Galveston, TX 77555

Edited by Lily Yeh Jan, University of California, San Francisco, CA, and approved February 28, 2020 (received for review October 11, 2019)

**Although major depressive disorder (MDD) is highly prevalent, its pathophysiology is poorly understood. Recent evidence suggests that glycogen-synthase kinase 3 $\beta$  (GSK3 $\beta$ ) plays a key role in memory formation, yet its role in mood regulation remains controversial. Here, we investigated whether GSK3 $\beta$  activity in the nucleus accumbens (NAc) is associated with depression-like behaviors and synaptic plasticity. We performed whole-cell patch-clamp recordings of medium spiny neurons (MSNs) in the NAc and determined the role of GSK3 $\beta$  in spike timing-dependent long-term potentiation (tLTP) in the chronic unpredictable mild stress (CUMS) mouse model of depression. To assess the specific role of GSK3 $\beta$  in tLTP, we used *in vivo* genetic silencing by an adeno-associated viral vector (AAV2) short hairpin RNA against GSK3 $\beta$ . In addition, we examined the role of the voltage-gated potassium Kv4.2 subunit, a molecular determinant of A-type K<sup>+</sup> currents, as a potential downstream target of GSK3 $\beta$ . We found increased levels of active GSK3 $\beta$  and augmented tLTP in CUMS mice, a phenotype that was prevented by selective GSK3 $\beta$  knockdown. Furthermore, knockdown of GSK3 $\beta$  in the NAc ameliorated depressive-like behavior in CUMS mice. Electrophysiological, immunohistochemical, biochemical, and pharmacological experiments revealed that inhibition of the Kv4.2 channel through direct phosphorylation at Ser-616 mediated the GSK3 $\beta$ -dependent tLTP changes in CUMS mice. Our results identify GSK3 $\beta$  regulation of Kv4.2 channels as a molecular mechanism of MSN maladaptive plasticity underlying depression-like behaviors and suggest that the GSK3 $\beta$ -Kv4.2 axis may be an attractive therapeutic target for MDD.**

GSK3 $\beta$  | Kv4.2 | chronic stress | depression | spike timing-dependent plasticity

**M**ajor depressive disorder (MDD) is a debilitating disease affecting ~16% of the world's population (1). MDD is characterized by low mood, lack of interest in outside stimuli, loss of concentration, hopelessness, and increased suicide risk (1, 2). Although the etiology and pathophysiology of MDD remain unclear, strong evidence indicates that brain region-specific changes in signaling pathways, neuroplasticity, neuroinflammation, and neurometabolites are primarily involved (3). Specifically, alterations in the nucleus accumbens (NAc) circuitry—part of the reward circuit—are thought to play a key role in MDD (4). However, to date, the molecular and cellular mechanisms underlying altered neuronal plasticity of the NAc associated with depression-like behaviors remain unclear.

GSK3 is a serine/threonine kinase ubiquitously expressed in eukaryotes (5). The GSK3 $\beta$  isoform is highly enriched in the brain (6), contributing to synaptic transmission (7), synaptic plasticity (8), gene expression (9), neurogenesis (10), and apoptosis (11). While dysregulation of GSK3 $\beta$  activity has been implicated in schizophrenia (12), Alzheimer's disease (13), and addictive behaviors (14), stabilizing GSK3 $\beta$  function has become the gold

standard for pharmacological treatment of mood disorders (15), providing clinical evidence for an intimate link between the kinase and mood regulation.

GSK3 $\beta$  is constitutively active and subject to inhibitory control through phosphorylation of Ser-9 by upstream protein kinases, such as Akt, protein kinase A (PKA), and protein kinase C, a mechanism that results in disinhibition of the kinase upon dephosphorylation of Ser-9 (16). GSK3 $\beta$  has been demonstrated to be important in regulation of synaptic plasticity. Indeed, unlike other serine/threonine kinases, GSK3 $\beta$  activity is suppressed during long-term potentiation (LTP) and required for long-term depression (LTD) induction (17), suggesting a unique role of this enzyme in synaptic plasticity.

Building on this evidence, we posited that alterations of synaptic plasticity induced by GSK3 $\beta$  signaling could be a causative link and a converging mechanism underlying depression-like behaviors in animal models.

To test this hypothesis, we studied the role of GSK3 $\beta$ -dependent modulation of spike timing-dependent plasticity (STDP) in medium spiny neurons (MSNs) of the NAc shell of mice exposed to chronic unpredictable mild stress (CUMS), a well-established model of depression (18). Although the most studied forms of synaptic plasticity in the NAc are classical LTP and LTD, we focus on STDP, in which the direction and degree of synaptic

## Significance

**GSK3 $\beta$  is a serine/threonine kinase highly expressed in the brain that regulates several ion channels and receptors. Our study uncovers increased levels of active GSK3 $\beta$  in the nucleus accumbens (NAc) of mice with a depressive-like phenotype induced by chronic stress. We clarify that the increased levels of active GSK3 $\beta$  within the NAc of these mice lead to altered synaptic plasticity through phosphorylation of the Kv4.2 subunit, a molecular determinant of A-type K<sup>+</sup> currents. Moreover, selective GSK3 $\beta$  silencing in the NAc prevents maladaptive synaptic plasticity and depression-related behavior, paving the way to consider the GSK3 $\beta$ -Kv4.2 axis as a strategy to manage the negative impact of chronic stress.**

Author contributions: G.A., F.L., M.D., and C.G. designed research; G.A., C.C., L.L., S.F., M.R., and F.S. performed research; T.A.G. contributed new reagents/analytic tools; G.A. and M.D. analyzed data; and M.D. and C.G. wrote the paper.

The authors declare no competing interest.

This article is a PNAS Direct Submission.

Published under the PNAS license.

<sup>1</sup>To whom correspondence may be addressed. Email: marcello.dascenzo@unicatt.it.

<sup>2</sup>M.D. and C.G. contributed equally to this work.

This article contains supporting information online at <https://www.pnas.org/lookup/suppl/doi:10.1073/pnas.1917423117/-DCSupplemental>.

First published March 24, 2020.

modification are determined by the coherence of pre- and post-synaptic activities within a neuron (19–21), because this form of plasticity is particularly relevant in the NAc, where MSNs typically fire and receive glutamatergic inputs at low frequencies (1 to 10 Hz) (22–24). Furthermore, STDP is generally recognized as a leading cellular mechanism for behavioral learning and memory with high computational properties, and growing evidence indicates that this mechanism may also play an important role in the pathogenesis of brain disorders including neuropsychiatric disorders (19).

## Results

**CUMS Treatment Affects Timing-Dependent LTP in Shell Accumbens Medium Spiny Neurons.** Electrophysiological recordings in acute slices of the NAc shell were performed with the whole-cell patch-clamp technique from visually identified MSNs, which represent >95% of the neurons in this brain region. In addition to morphological criteria, MSNs were identified based on previously defined electrophysiological parameters (25, 26). In some experiments, cells were filled with biocytin and morphologically reconstructed for further validation (Fig. 1 *A* and *B*).

Excitatory postsynaptic potentials (EPSPs) were evoked using extracellular stimulation at a frequency of 0.2 Hz. We paired postsynaptic action potentials (APs) and EPSPs evoked with a 20-ms interval at a rate of 1 Hz (90 times; Fig. 1*C*) to generate synaptic plasticity. In 52.9% of MSNs tested, EPSP slope after pairing was significantly increased compared with baseline (Fig. 1*C* and *D*). EPSP slope potentiation lasted the entire recording session (~40 min) and was ascribed as timing-dependent long-term potentiation (tLTP). In the remaining MSNs tested (47.1%), the same stimulation paradigm evoked a significant depression (Fig. 1*E* and *F*; timing-dependent long-term depression; tLTD). The observed ability of the same AP–EPSP pairing protocol to induce tLTP and tLTD in about equal proportions in the NAc MSNs is in accordance with previous studies (21, 27) and is a marked departure from other brain regions such as the CA1 hippocampus and prefrontal cortex, where the pairing order determines plasticity direction (20).

We exposed male mice to 3 wk of the CUMS protocol and compared tLTP amplitude with those of control mice to determine whether stress exposure affected the above-reported STDP. A depressive-like phenotype in CUMS mice was validated by using the forced swim test (FST) (28), sucrose preference test (SPT) (29), and elevated plus maze (EPM) (30) (Fig. 2*B–D*). In CUMS mice, tLTP amplitude was significantly greater than in control mice (Fig. 2*E* and *F*). Furthermore, in CUMS mice, tLTP was observed much more frequently than tLTD (tLTP/tLTD ratio 1.8; Fig. 2*G*). These results indicate that the CUMS protocol caused a significant tLTP modulation together with a shift of the tLTP/tLTD ratio favoring tLTP.

**Knocking Down GSK3 $\beta$  in MSNs Counteracts CUMS-Induced Changes in tLTP.** GSK3 $\beta$  activation, via decreased inhibitory phosphorylation at serine 9, was reported in the brains of mice exhibiting learned helplessness (31) as well as in the NAc of mice exhibiting depression-like behaviors following social defeat stress (32). These findings support the notion that increased levels of active GSK3 $\beta$  may promote depression-like behavior.

Consistently, we found that in the NAc of CUMS-treated mice, GSK3 $\beta$  activity was enhanced by decreased Ser-9 phosphorylation. Indeed, Western blot analysis of NAc cell lysates showed decreased levels of pGSK3 $\beta$ <sup>Ser-9</sup> in CUMS mice with no significant changes in total GSK3 $\beta$  (Fig. 2*H* and *I*). We also found an increase of GSK3 $\beta$  phosphorylation (Fig. 2*H* and *I*) at the tyrosine 216 activating site (33–35). To confirm that CUMS treatment actually involves an alteration in GSK3 $\beta$  enzymatic activity in the NAc and to quantify this change, we measured the GSK3 $\beta$  activity of the homogenates using fluorescent gel shift

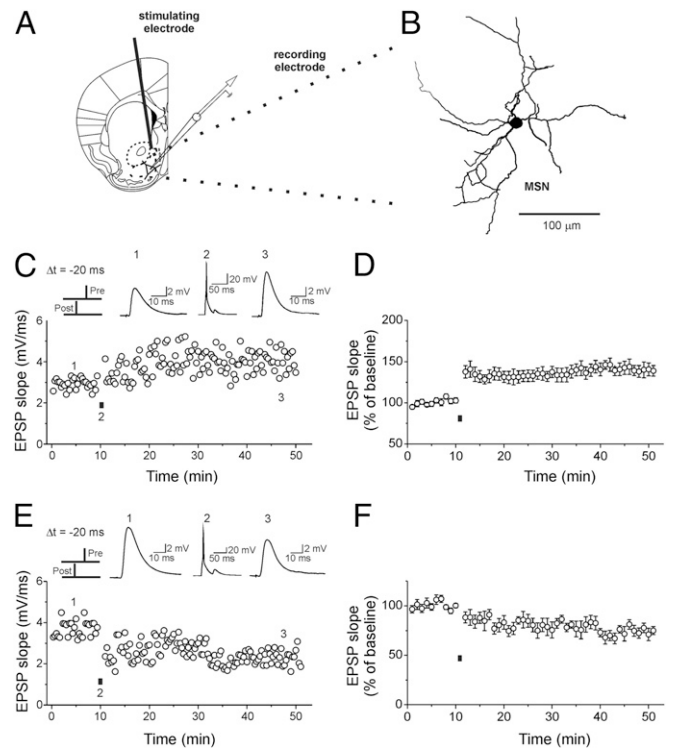


**Fig. 1.** Equivalent AP–EPSP pairing conditions evoke both tLTP and tLTD in MSNs of the NAc shell. (*A*) Schematic diagram of a brain section at NAc shell level with the patch pipette located in the MSN soma and the stimulating electrode positioned 200 to 300  $\mu$ m dorsal to the recording electrode. (*B*) Z-stack acquisition of a morphologically recovered MSN within the shell of the NAc. (*C*) The induction protocol for STDP is depicted (*Top Left*). A single AP, elicited by current injections into the postsynaptic neuron (Post), was paired with a following EPSP evoked by extracellular stimulation (Pre). The AP preceded the onset of the EPSP by  $\Delta t = -20$  ms. Representative traces of evoked EPSPs in controls (1), during pairings with an AP (2), and after conditioning (3) are shown (*Top, Middle* and *Right*). The EPSP slope for the entire experiment is shown (*Bottom*). A horizontal black bar indicates the pairing period (90 episodes at 1 Hz). (*D*) Normalized mean  $\pm$  SEM for 9 experiments in which tLTP was elicited ( $135.8 \pm 6.8\%$  of baseline; from four mice). (*E*) tLTD in an MSN using the same induction protocol shown in *C*. (*F*) Normalized mean  $\pm$  SEM for 9 experiments in which tLTD was elicited ( $75.4 \pm 2.9\%$  of baseline; from four mice). In all experiments, resting membrane potentials and input resistance did not change by >20%.

electrophoresis (36). As reported in *SI Appendix, Fig. S1B*, there was a significant increase in kinase activity compared with that of control mice.

We then hypothesized that knocking down GSK3 $\beta$  in NAc MSNs would counteract the increased tLTP in mice exposed to CUMS. To test our hypothesis, we used *in vivo* genetic silencing by injecting an adeno-associated viral vector (AAV2) short hairpin RNA against mouse GSK3 $\beta$  (AAV-shGSK3 $\beta$ -GFP [green fluorescent protein]) into the NAc shell of adult mice (37, 38). AAV-shCTRL-GFP not targeting any known mouse transcripts was used as control (37). The genetic silencing procedure was validated in our experimental model by assessing GSK3 $\beta$  messenger RNA (mRNA) levels with a recently developed protocol that combines whole-cell patch-clamp recordings with high-quality single-cell reverse-transcription quantitative real-time PCR (39, 40). *SI Appendix, Fig. S2* shows that the amount of GSK3 $\beta$  mRNA was strongly reduced in MSNs where the GSK3 $\beta$  shRNA construct was expressed compared with the control hairpin.

In accordance with our hypothesis, tLTP slope was significantly reduced in MSNs of mice transfected with AAV-shGSK3 $\beta$  and exposed to the CUMS protocol (Fig. 3*B* and *C*). Furthermore, the

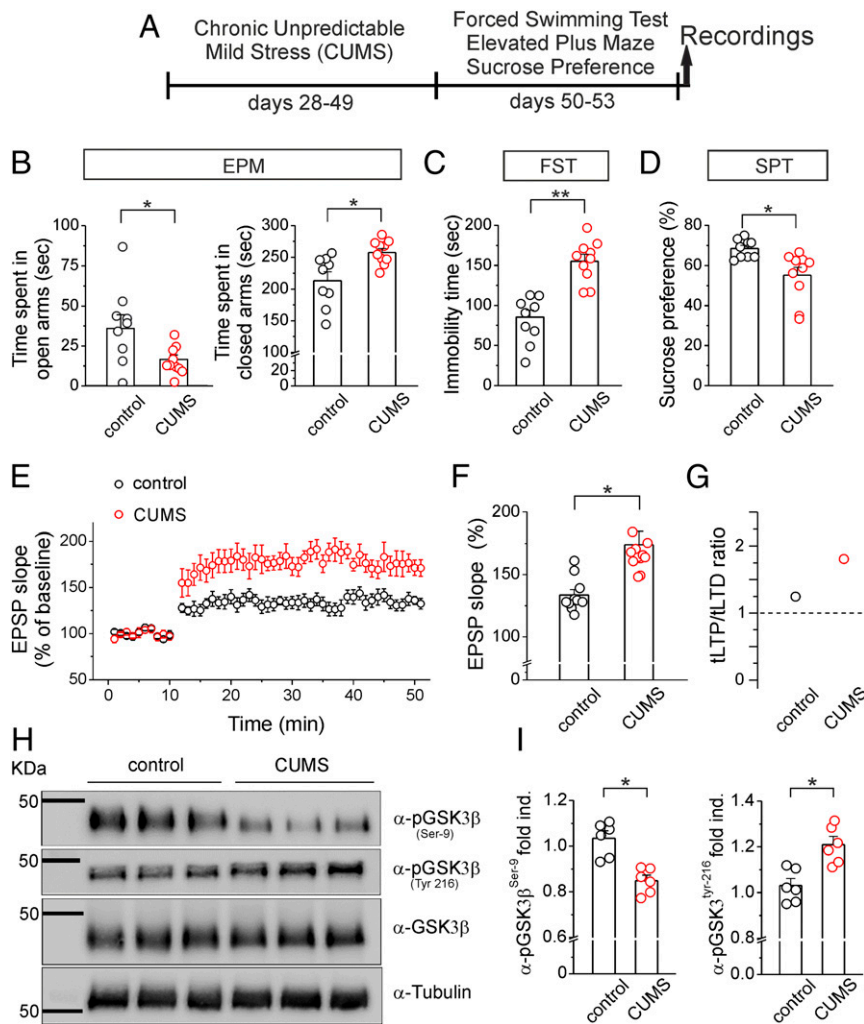


**Fig. 2.** Increased tLTP amplitude in MSNs of CUMS mice is associated with enhanced levels of active GSK3 $\beta$ . Male C57/BL6 mice were exposed to chronic unpredictable mild stress. (A) Experimental timeline. (B–D) CUMS-treated mouse and control mouse behaviors in EPMs, FSTs, and SPTs [control,  $n = 9$ ; CUMS,  $n = 10$ ; EPM open arm:  $35.8 \pm 8.6$  versus  $16.6 \pm 2.8$  s; one-way ANOVA;  $F_{(2,19)} = 6.3$ ;  $P < 0.05$ ; followed by Tukey post hoc test;  $*P < 0.05$ ; EPM closed arm:  $212.9 \pm 14.1$  versus  $257.7 \pm 6.3$  s; one-way ANOVA;  $F_{(2,19)} = 8.0$ ;  $P < 0.05$ ; followed by Tukey post hoc test;  $**P < 0.01$ ; SPT:  $68.4 \pm 1.6\%$  versus  $55.1 \pm 3.9\%$ ; one-way ANOVA;  $F_{(2,19)} = 9.6$ ;  $P < 0.001$ ; followed by Tukey post hoc test;  $*P < 0.05$ ]. (E) Time course of EPSP slope, normalized to baseline values, showing that tLTP amplitude is increased in MSNs of CUMS-treated mice (red circles;  $n = 11$  from five mice) compared with control mice [open circles;  $n = 10$  from five mice; one-way ANOVA;  $F_{(2,21)} = 35.1$ ; followed by Tukey post hoc test;  $P < 0.05$ ]. (F) Bar graph comparing the average EPSP slope under the experimental conditions shown in E. (G) Ratio between the numbers of MSNs exhibiting tLTP or tLTD in control and CUMS-treated mice;  $*P < 0.05$ . (H and I) Representative Western blots of NAc tissue showing decreased levels of GSK3 $\beta$  phosphorylated at Ser-9 and increased levels of GSK3 $\beta$  phosphorylated at Thy-216 in CUMS-treated mice ( $n = 6$  from six mice; statistics by Mann–Whitney  $U$  test;  $*P < 0.05$ ). Error bars represent SEM,  $*P < 0.05$ ,  $**P < 0.01$ .

tLTP/tLTD ratio was close to 1, pointing to equal probability of evoking tLTP and tLTD (Fig. 3D). These results indicate that knocking down GSK3 $\beta$  in NAc MSNs counteracts CUMS-induced changes in STDP.

**Pharmacological Agents Affecting GSK3 Activity and GSK3 $\beta$  Knockdown Regulate tLTP in MSNs.** To corroborate the above-reported results, we tested pharmacological modulation of GSK3 $\beta$  on AP–EPSP pairing-induced STDP in control mice. First, we used the highly selective GSK3 inhibitor CT-99021 (1  $\mu$ M) (41–45) that was injected into the recorded MSN via a patch pipette. Under these experimental conditions, tLTP was significantly decreased compared with what we observed following intracellular perfusion with the vehicle (DMSO; 1/1,000 dilution) (SI Appendix, Fig. S3 A and B).

N-terminal phosphorylation at Ser-9, induced by protein kinase B type 1 (Akt-1), inhibits GSK3 activity (41, 46). We therefore

speculated that pharmacological inhibition of Akt-1 would lead to increased tLTP through an increased GSK3 $\beta$  activation. In support of this hypothesis, we found that when the Akt-1 inhibitor triciribine (10  $\mu$ M) was intracellularly perfused into MSNs, tLTP slope was significantly increased compared with controls (SI Appendix, Fig. S3 A and B). Accordingly, triciribine administration reduced inhibitory phosphorylation of GSK3 $\beta$  on Ser-9 (SI Appendix, Fig. S4). Finally, we hypothesized that knocking down GSK3 $\beta$  in MSNs would result in decreased tLTP similar to what we observed after pharmacological GSK3 inhibition. As shown in SI Appendix, Fig. S3 D and E, pairing stimulation-induced tLTP was less pronounced in neurons transfected with AAV-shGSK3 $\beta$  compared with controls. In addition, we found that the tLTP/tLTD ratio was also influenced by pharmacological agents affecting GSK3 activity and by GSK3 $\beta$  knockdown (SI Appendix, Fig. S3 C and F). Taken together, these results indicate that active GSK3 $\beta$  inversely regulates tLTP magnitude in MSNs of the NAc



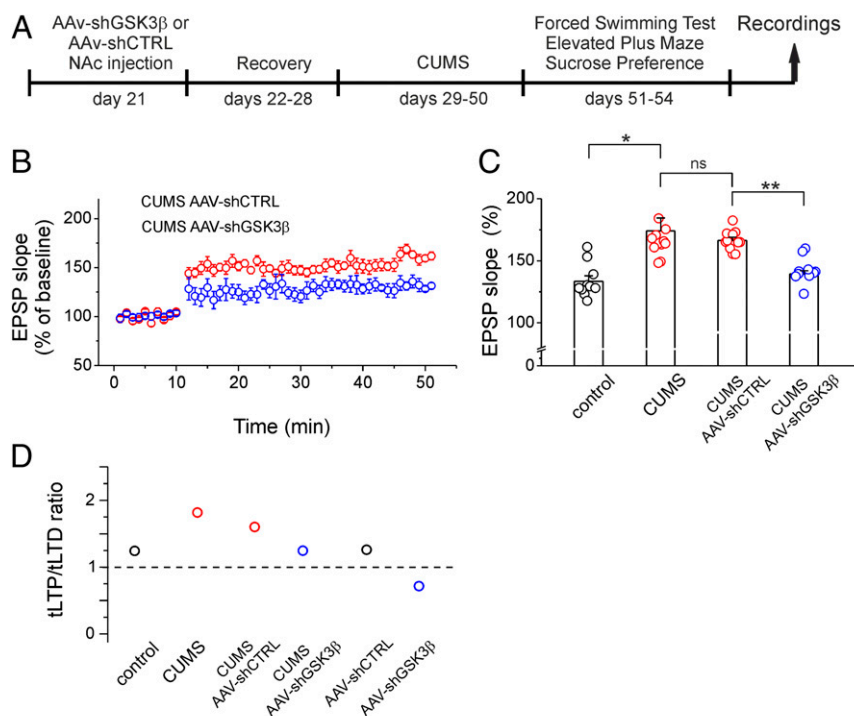


**Fig. 3.** Knockdown of GSK3 $\beta$  in the NAc counteracts CUMS-induced changes in tLTP. (A) Experimental timeline. (B) Time course of EPSP slope showing that tLTP was significantly reduced in MSNs from CUMS-treated mice transfected with a vector designed to knock down GSK3 $\beta$  (AAV-shGSK3 $\beta$ ; blue circles;  $n = 10$  from five mice) compared with tLTP measured in MSNs transfected with control vector [AAV-shCTRL; red circles;  $n = 11$  from six mice; one-way ANOVA;  $F_{(2,21)} = 59.1$ ;  $P < 0.05$ ; followed by Tukey post hoc test;  $P < 0.05$ ]. (C) Bar graph comparing the average EPSP slope under the experimental conditions shown in B;  $**P < 0.01$ . For comparison, tLTP in CUMS and control mice is also shown (the same data are shown in Fig. 2F). Note that the tLTP slope in MSNs from CUMS-treated mice transfected with control vector was comparable to that of CUMS mice. ns, not significant. (D) Ratio between the numbers of MSNs exhibiting tLTP or tLTD in the four experimental conditions. The tLTP/tLTD ratio in mice injected with AAV-shGSK3 $\beta$  and AAV-shCTRL is also shown for comparison (see also *SI Appendix, Fig. S3*). Error bars represent SEM,  $*P < 0.05$ ,  $**P < 0.01$ .

shell and support our findings of GSK3 $\beta$ -dependent change in tLTP occurring in CUMS-treated mice.

**Knockdown of GSK3 $\beta$  in the NAc Shell Ameliorates Depressive-Like Behaviors in CUMS Mice.** To determine whether altered GSK3 $\beta$  signaling contributed to CUMS-induced depressive-like behavior, we compared EPM, FST, and SPT values in mice transfected with either AAV-shGSK3 $\beta$  or AAV-shCTRL-GFP before being exposed to the CUMS protocol.

As expected, mice transfected with AAV-shCTRL-GFP and subjected to the CUMS protocol showed depressive-like behavior (Fig. 4): In the EPM test, they spent significantly less time in the open arm and longer time in the closed arm than control mice transfected with AAV-shCTRL-GFP (Fig. 4B). Accordingly, FST and SPT also revealed a depressive-like phenotype in CUMS mice transfected with AAV-shCTRL-GFP (Fig. 4C and D). Interestingly, when mice were transfected with AAV-shGSK3 $\beta$  and exposed to the CUMS protocol, their behavioral phenotype was similar to that we observed in control mice and significantly different from CUMS mice transfected with AAV-shCTRL-GFP, characterized by a depressive-like phenotype. It is important to note that no difference in locomotor activity was found between mice transfected with AAV-shGSK3 $\beta$  and AAV-shCTRL-GFP (*SI Appendix, Fig. S5*), in accordance with a previous study performed in rats (37).

Because modulation of NAc shell circuitry affects depression-related behaviors (47), our finding that knockdown of GSK3 $\beta$  in CUMS mice prevents a depressive-like phenotype suggests that GSK3 $\beta$  signaling dysfunction is a molecular correlate of CUMS-induced depressive-like behaviors.

**An A-Type K $^+$  Current Mediated by Kv4.2 Channels Is Highly Expressed in MSNs of the NAc Shell.** We next sought to identify the molecular mechanism downstream of GSK3 $\beta$  underlying the STDP modulation we observed in CUMS-treated mice. In a recent study, we demonstrated a functional interaction between GSK3 $\beta$  and voltage-gated potassium Kv4.2 channels, molecular determinants of A-type K $^+$  currents, as a novel mechanism for synaptic plasticity modulation in layer 2/3 pyramidal neurons of the somatosensory cortex (38). As A-type K $^+$  currents are critical for dendritic and synaptic processing during synaptic plasticity (48), we hypothesized that GSK3 $\beta$ -dependent inhibition of Kv4.2 channels in mice exposed to CUMS would lead to broadened dendritic back-propagation, increased Ca $^{2+}$  influx during the pairing protocol, and, as a consequence, increased tLTP.

In the mouse brain, Kv1.4, Kv3.3, Kv3.4, and all members of Kv4 channel subfamilies can generate A-type K $^+$  currents (49). However, the molecular entity generating A-type transient K $^+$  current in MSNs of the NAc has not been identified yet. Therefore, we first attempted to relate the biophysical and pharmacological properties of this current to a channel subtype(s).

Whole-cell voltage-clamp recordings of the outward currents in response to voltage steps ranging from  $-110$  to  $+40$  mV revealed an early A-type K $^+$  current which could be isolated by applying a prepulse protocol (50–52) (*Materials and Methods*) in the presence of 20 mM tetraethylammonium (TEA) to suppress slower K $^+$  currents (Fig. 5A–C).

The steady-state activation and inactivation relationship (Fig. 5D), as well as its recovery from inactivation (Fig. 5E), was determined using the protocols shown in Fig. 5. The peak conductance–voltage relationship ( $G_p$ – $V$  curve) was described by a first-order Boltzmann

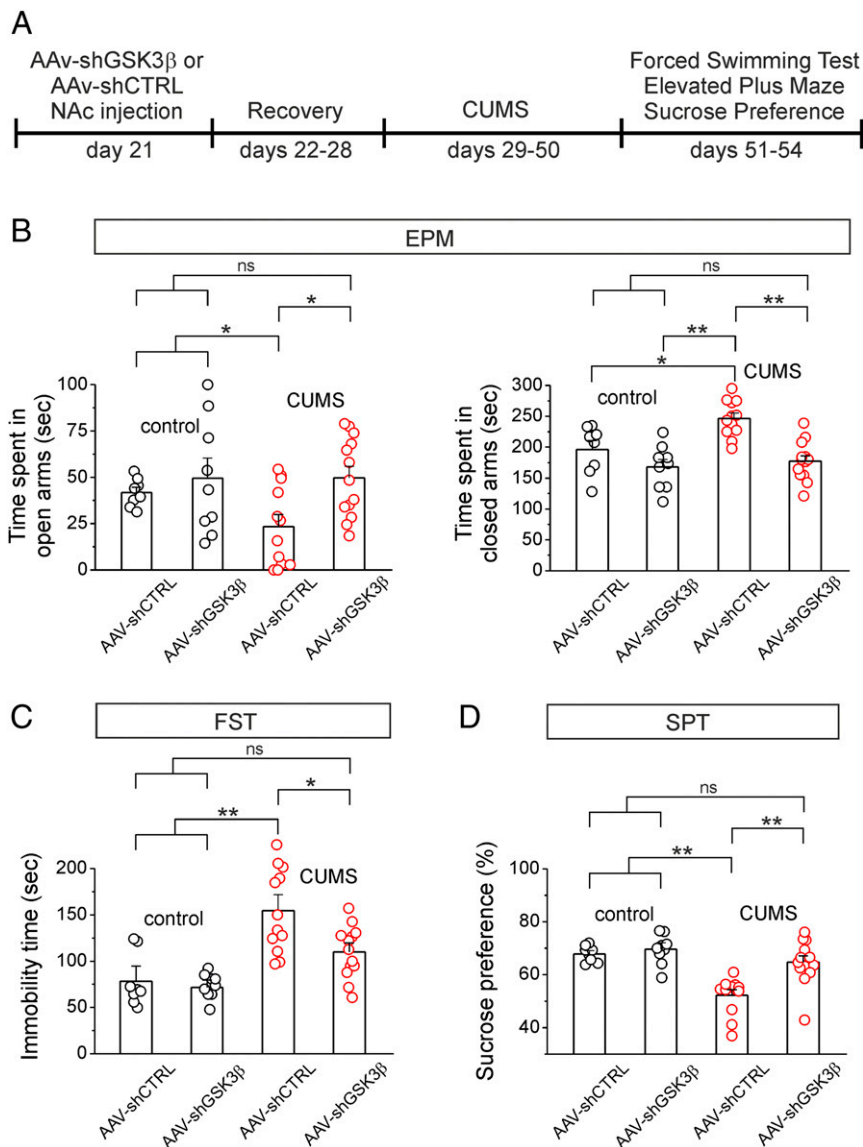


**Fig. 4.** Knockdown of GSK3 $\beta$  in the NAc ameliorates depressive-like behavior in mice exposed to the CUMS protocol. (A) Experimental timeline. (B–D) Behavioral analysis by EPMs, FSTs, and SPTs of CUMS and control mice in which NAc was injected with either the AAV-shGSK3 $\beta$  or AAV-shCTRL virus vector. Note that mice exposed to the CUMS protocol and transfected with AAV-shCTRL showed a depressive-like phenotype compared with control AAV-shCTRL mice [EPM open arm:  $23.4 \pm 6.4$  versus  $41.8 \pm 2.9$  s; one-way ANOVA;  $F_{(2,20)} = 5.3$ ;  $P < 0.05$ ; followed by Tukey post hoc test;  $*P < 0.05$ ; EPM closed arm:  $246.5 \pm 8.8$  versus  $196.3 \pm 16.4$  s; one-way ANOVA;  $F_{(2,20)} = 10.9$ ;  $P < 0.05$ ; followed by Tukey post hoc test;  $*P < 0.05$ ;  $n = 12$  and  $8$ , respectively; FST:  $154.5 \pm 17.4$  versus  $78.1 \pm 16.7$  s; one-way ANOVA;  $F_{(2,20)} = 17.4$ ;  $P < 0.001$ ; followed by Tukey post hoc test;  $**P < 0.001$ ;  $n = 8$  and  $12$ , respectively; SPT:  $52.3 \pm 2.0\%$  versus  $67.9 \pm 1.1\%$ ; one-way ANOVA;  $F_{(2,20)} = 5.9$ ;  $P < 0.001$ ; followed by Tukey post hoc test;  $**P < 0.01$ ;  $n = 8$  and  $12$ , respectively]. The behavioral phenotype was significantly different in mice exposed to the CUMS protocol transfected with AAV-shGSK3 $\beta$  compared with CUMS AAV-shCTRL mice [EPM open arm:  $49.8 \pm 2.9$  versus  $23.4 \pm 6.4$  s; one-way ANOVA;  $F_{(2,25)} = 9.4$ ;  $P < 0.05$ ; followed by Tukey post hoc test;  $*P < 0.05$ ; EPM closed arm:  $177.1 \pm 9.1$  versus  $246.5 \pm 8.8$  s; one-way ANOVA;  $F_{(2,25)} = 32.3$ ;  $P < 0.001$ ; followed by Tukey post hoc test;  $**P < 0.01$ ; FST:  $105.9 \pm 17.4$  versus  $154.5 \pm 17.4$  s; one-way ANOVA;  $F_{(2,25)} = 8.7$ ;  $P < 0.05$ ; followed by Tukey post hoc test;  $*P < 0.05$ ; SPT:  $64.7 \pm 2.0\%$  versus  $52.3 \pm 2.0\%$ ; one-way ANOVA;  $F_{(2,25)} = 48.3$ ;  $P < 0.001$ ; followed by Tukey post hoc test;  $**P < 0.01$ ;  $n = 13$  and  $12$ , respectively]. ns, not significant. Error bars represent SEM,  $*P < 0.05$ ,  $**P < 0.01$ .

function with an activation midpoint ( $V_{1/2}$ ) of  $-4.6 \pm 1.8$  mV ( $n = 22$ ). A first-order Boltzmann function with an average half-inactivation voltage ( $V_{1/2i}$ ) of  $-38.5 \pm 0.8$  mV ( $n = 14$ ) described the steady-state inactivation curve.

The values of  $V_{1/2}$  and  $V_{1/2i}$  of A-type K $^{+}$  current we found suggested that this current is likely not carried by Kv3.3 and Kv3.4 channels, which activate and inactivate at more depolarizing potentials (53). Recovery from inactivation was examined by using a two-pulse protocol (Fig. 5). Peak current amplitudes after each recovery time were normalized to the maximal amplitude and plotted as a function of recovery time. These data were fitted by

the sum of two exponentials with a weighted recovery time constant of  $27.7 \pm 11.0$  ms ( $n = 10$ ). This finding allowed us to exclude that Kv1.4 channels contributed to the A-type K $^{+}$  current recorded in MSNs of the NAc shell because the time constant for recovery from inactivation of these channel subtypes is in the range of seconds (53, 54). The gating properties of the recorded channels closely resemble those of the Kv4 family in different brain areas (53, 55, 56), and biophysical characterization was further supported by pharmacology. Indeed, the A-type K $^{+}$  current in NAc MSNs was very sensitive to local perfusion of 4 mM 4-AP, which is a nonspecific Kv4 blocker (Fig. 5 F and G; mean reduction of 87%;

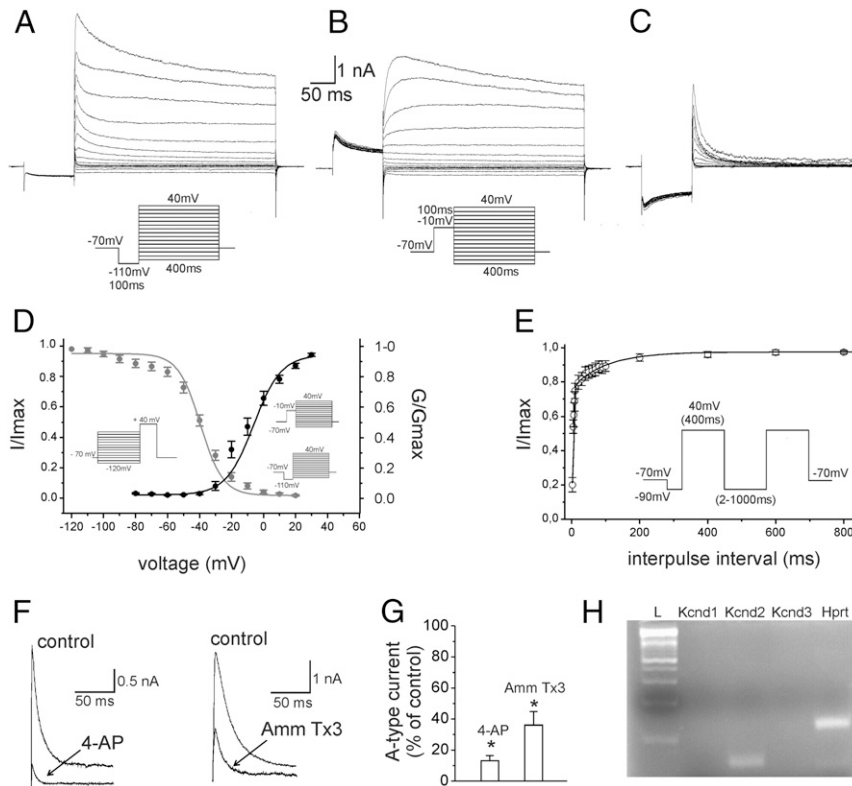


**Fig. 5.** Isolation and characterization of A-type  $K^+$  currents in MSNs of the NAC shell. (A) Whole-cell voltage-clamp recording of the outward currents evoked by a series of depolarizing steps from  $-110$  to  $+40$  mV following a hyperpolarizing step to  $-110$  mV to enable maximal  $K^+$  conductance (holding potential  $-70$  mV). (A, *Inset*) Voltage protocols. (B) A prepulse to  $-10$  mV (100 ms) was applied before the voltage steps to inactivate the transient  $K^+$  channels. (B, *Inset*) Voltage protocols. (C) The transient A-type  $K^+$  currents were isolated by digitally subtracting the currents in B from those in A. The recordings of isolated A-type  $K^+$  currents in MSNs were obtained after a 10-min perfusion of ACSF containing  $1 \mu\text{M}$  TTX,  $300 \mu\text{M}$   $\text{Cd}^{2+}$ , and  $20$  mM TEA. (D) Voltage dependence of A-type  $K^+$  current activation and inactivation. The activation (black circles;  $n = 22$  from seven mice) and steady-state inactivation (gray circles;  $n = 15$  from six mice) curves were fitted using a first-order Boltzmann function. (D, *Inset*s) Protocols used to determine the voltage dependence of A-type  $K^+$  current activation and inactivation. (E) Recovery from inactivation of A-type  $K^+$  current. The time course of recovery from inactivation was fitted with the sum of two exponentials from data obtained in 10 neurons (from four mice) using the double protocol shown (*Inset*). (F) Representative traces showing  $K^+$  currents before and after treatment with  $4$  mM 4-AP (*Left*), an A-type channel blocker, and  $500$  nM AmmTX3, a more selective inhibitor of Kv4.2 channels (*Right*). (G) Bar graph showing the average current reductions after perfusion of 4-AP and AmmTX3;  $*P < 0.05$ . (H) Representative gel showing the products of single-cell qRT-PCR transcript expression of Kv4 subunits in addition to the housekeeping gene Hprt from the same MSN. The first lane (L) represents a DNA ladder. Primers used in this experiment were validated by qRT-PCR performed on cDNA obtained from total mouse cortex tissue extract (*SI Appendix, Fig. S6*). Error bars represent SEM,  $*P < 0.05$ .

$n = 7$ ). Lastly, we tested the specific Kv4 channel blocker AmmTX3 ( $500$  nM) (50, 57) and observed a mean reduction of  $64\%$  (Fig. 5 F and G;  $n = 8$ ) in the peak current amplitude, suggesting the Kv4 identity of the recorded A-type  $K^+$  current.

To corroborate the electrophysiological data, we profiled the expression of Kv4 channel subunits by using a protocol that combines whole-cell patch-clamp recordings with high-quality single-cell RNA sequencing. To assess the presence of mRNA transcripts for Kv4.1, Kv 4.2, Kv 4.3, and the housekeeper gene Hprt single-cell qRT-PCR was performed on 18 MSNs. Fig. 5H shows a representative example of a gel showing bands for one of the three Kv4 subunits and Hprt. Typically, we observed that the vast majority of MSNs were positive for the Kv4.2 subtype (17/18, 94.4%), whereas only two MSNs expressed both Kv4.2 and Kv4.3 transcripts (2/18, 11.1%). We never observed Kv4.1 mRNA expression in all MSNs analyzed. The prevailing expression of Kv4.2 in MSNs of the NAC shell indicates that the A-type  $K^+$  current is mainly carried by this channel subtype.

**Reduced Kv4.2 Function in Mice Exposed to CUMS.** We next performed whole-cell patch-clamp recordings and compared the magnitude of A-type  $K^+$  currents in control and CUMS-treated mice. We speculated that in the NAC MSNs of CUMS-treated mice the

increased levels of active GSK3 $\beta$  would result in a decreased Kv4.2 channel activity through GSK3 $\beta$ -dependent phosphorylation at Ser-616 of the Kv4.2 subunit. In support of this hypothesis, we found that in CUMS mice the A-type  $K^+$  current density was lower than that observed in control mice (Fig. 6 A and B). Specifically, CUMS mice displayed a more depolarized activation voltage and a slower rate of recovery from inactivation compared with control mice (*SI Appendix, Fig. S7*). We also found that the inactivation curve was not shifted in CUMS mice. To gain insight into the phosphorylation-dependent regulation of the Kv4.2 channel by GSK3 $\beta$ , we also performed Western blot analysis of the total NAC tissue lysate to examine the phosphorylation levels of Ser-616 in control and CUMS mice. As shown in Fig. 6 C and D, CUMS treatment led to a significant increase ( $P < 0.05$ ) in Ser-616 phosphorylation levels compared with control mice (for validation of the anti-Kv4.2 antibody, see *SI Appendix, Fig. S8*). In addition, in mice exposed to the CUMS protocol and transfected with AAV-shGSK3 $\beta$ , the A-type  $K^+$  current density was similar to what was observed in MSNs of control mice (Fig. 6 A and B), an effect that was associated with a shift in the activation voltage to more hyperpolarized voltages (*SI Appendix, Fig. S7 B and C*). In accordance with these results, we also observed that pharmacological

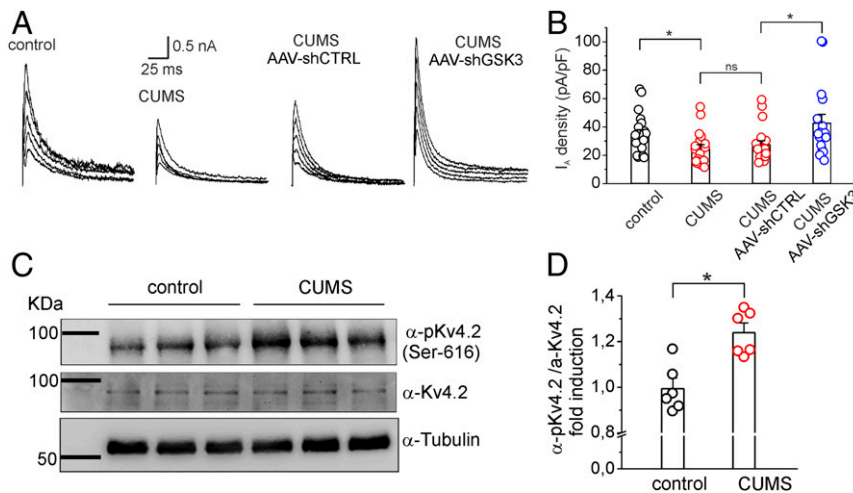


**Fig. 6.** A-type  $K^+$  current is down-regulated in MSNs of CUMS-treated mice, an effect that is counteracted by GSK3 $\beta$  knockdown. (A) Representative traces showing transient A-type  $K^+$  currents recorded at different voltages in MSNs from control (Left), CUMS mice, and CUMS-treated mice and transfected with AAV-shGSK3 $\beta$  and AAV-shCTRL (Right). (B) Bar graph showing decreased A-type  $K^+$  current densities in MSNs from control and CUMS-treated mice [current recorded at +40 mV; CUMS mice:  $23.7 \pm 2.9$  pA/pF;  $n = 19$  from six mice; control mice:  $34.7 \pm 3.4$  pA/pF;  $n = 19$  from seven mice; one-way ANOVA;  $F_{(2,38)} = 4.9$ ;  $P < 0.05$ ; followed by Tukey post hoc test;  $*P < 0.05$ ]. The bar graph also shows increased current density in CUMS AAV-shGSK3 $\beta$  mice compared with CUMS AAV-shCTRL [one-way ANOVA;  $F_{(2,35)} = 35.7$ ;  $P < 0.001$ ; followed by Tukey post hoc test;  $*P < 0.05$ ;  $n = 17$  and  $18$  from  $5$  and  $6$  mice, respectively]. (C) Representative blots of the total cell lysate from NAc tissue probed with either anti-phospho-Ser-616 (Top) or total Kv4.2 (Middle) antibody in control and CUMS-treated mice. (D) Densitometry analysis for the blots probed with anti-phospho-Ser-616 and normalized to total Kv4.2 channels is shown ( $n = 6$  from six mice; statistics by Mann-Whitney  $U$  test;  $*P < 0.05$ ). ns, not significant. Error bars represent SEM,  $*P < 0.05$ .

agents affecting GSK3 activity and GSK3 $\beta$  knockdown resulted in A-type  $K^+$  current modulation (SI Appendix, Fig. S9).

GSK3 $\beta$ -Kv4.2 interaction in MSNs was also studied by performing a set of experiments aimed at determining whether these two proteins colocalize in the NAc. Confocal microscopy images showed overlapping immunofluorescence signals of GSK3 $\beta$  and Kv4.2 channels in the MSN soma (SI Appendix, Fig. S10), suggesting a possible physical interaction, which was further investigated by immunoprecipitation experiments with total NAc lysates. By using an anti-GSK3 $\beta$  antibody, this assay revealed that the Kv4.2 channel coimmunoprecipitated with GSK3 $\beta$  (SI Appendix, Fig. S10B). These results demonstrate that 1) GSK3 $\beta$  and Kv4.2 physically interact in the NAc shell, and 2) A-type  $K^+$  currents in MSNs of CUMS mice are down-regulated through GSK3 $\beta$ -dependent phosphorylation at the Ser-616 site. These findings were also corroborated by results of current-clamp experiments aimed at evaluating resting and active membrane properties of MSNs from CUMS and control mice. As reported in SI Appendix, Fig. S11, MSNs from CUMS mice show a broadening of the action-potential width, reduced first-spike latency, and increase in firing rate, all features that are consistent with a decrease in A-type  $K^+$  currents (58, 59).

**CUMS Protocol Ocludes the Effect of A-Type  $K^+$  Channel Inhibition on tLTP.** Data shown so far indicate that modulation of Kv4.2 channels may underlie GSK3 $\beta$  action on tLTP in CUMS-treated mice. To corroborate these findings, we performed a new set of experiments and compared the amplitude of tLTP in slices from CUMS mice in the presence or absence of the specific Kv4 channel blocker AmmTX3. We hypothesized that if a GSK3 $\beta$ -dependent increase in tLTP observed in CUMS mice is indeed due to chronic reduction of Kv4.2 channel activity, the pharmacological blockade of these channels would have no effect on tLTP recorded in slices from CUMS mice because of saturation of the signaling pathway. We first examined the effects of pharmacological A-type  $K^+$  current blockade on tLTP. As shown in Fig. 7, when 200 nM AmmTX3 was present in the bath, tLTP was significantly increased. It is noteworthy that at this concentration AmmTX3 reduced the A-type  $K^+$  current amplitudes by about

40% (50, 57), a level that still allows cell firing. Interestingly, the magnitude of the facilitatory effect of AmmTX3 on tLTP was similar to that observed in CUMS mice (Fig. 7A and B). We then performed occlusion experiments by recording tLTP in brain slices of CUMS mice perfused with AmmTX3. Importantly, under these experimental conditions, tLTP magnitude and tLTP/tLTD ratio were not significantly different from that obtained when AmmTX3 was applied to brain slices of control mice or when tLTPs were recorded in CUMS animals (Fig. 7). These findings are in agreement with our hypothesis that increased tLTP in CUMS mice may rely on GSK3 $\beta$ -dependent down-regulation of Kv4.2 channels.

Collectively, our results identify GSK3 $\beta$  regulation of Kv4.2 channels as a molecular mechanism of MSN maladaptive plasticity underlying depression-like behaviors in the CUMS model of depression.

## Discussion

Animal models provide an essential tool to understand the biology of depression (60). Previous studies have validated the CUMS paradigm as a reliable and robust model of depression (18, 61). Although chronic stress causes numerous impairments in mood cognition and memory and may play a role in the development of different brain diseases, the CUMS procedures have produced the most consistent results in terms of neurochemical, neuroendocrine, and neuroimmune alterations observed in depression. Furthermore, on a behavioral level, this model has proven to be the most used model in preclinical research on depression by helping to confirm the effectiveness of conventional antidepressants (62). Here, we used the CUMS protocol to investigate neuroadaptive mechanisms in the NAc underlying depression-like behaviors, focusing on molecular mechanisms that could account for maladaptive plasticity of MSNs, the primary output of the NAc. We found a form of altered synaptic plasticity in MSNs developing in response to the CUMS paradigm, which was prevented by GSK3 $\beta$  silencing. Specifically, we observed a significant increase in tLTP amplitude in CUMS animals compared with controls, a phenotype that we attributed to the GSK3 $\beta$ -dependent decrease of Kv4.2 channel activity through phosphorylation of the Ser-616 residue.



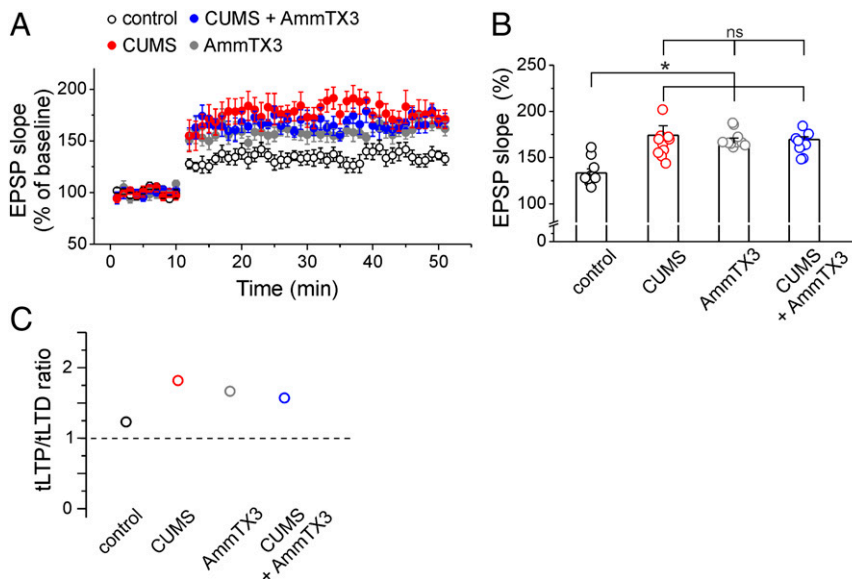


**Fig. 7.** Pharmacological A-type  $K^+$  channel inhibition increases tLTP in MSNs, an effect that is counteracted in CUMS mice. (A) Average time course of the EPSP slope during tLTP experiments in MSNs from control slices treated with 200 nM AmmTX3 (gray circles) and in MSNs recorded in slices obtained from CUMS animals and perfused with AmmTX3 (blue circles). For comparison, tLTPs recorded in control and CUMS mice are also shown (black and red circles, respectively; the same recordings are shown in Fig. 2A). Note that when AmmTX3 was present in the bath, tLTP was significantly increased compared with control experiments [one-way ANOVA;  $F_{(2,20)} = 23.7$ ;  $P < 0.05$ ; followed by Tukey post hoc test;  $*P < 0.05$ ;  $n = 10$  from five mice in both groups]. It is noteworthy that when AmmTX3 was perfused in slices from mice exposed to CUMS treatment, the magnitude of the tLTP was not significantly different from that obtained when AmmTX3 was applied alone (one-way ANOVA; followed by Tukey post hoc test;  $n = 11$ ;  $P > 0.5$ ) or when tLTPs were recorded in CUMS animals. (B) Bar graph depicting quantification of tLTP in the experimental conditions reported in A;  $*P < 0.05$ . (C) Ratio of MSN numbers evoking tLTP/tLTD in the experimental condition shown in A and B. ns, not significant. Error bars represent SEM,  $*P < 0.05$ .

Much experimental evidence supports our conclusion: 1) tLTP modulation in CUMS mice is associated with reduced Kv4.2 channel function; 2) pharmacological blockade of the A-type  $K^+$  channel mimics and occludes the CUMS-induced augmentation of tLTP; 3) NAc tissue of mice exposed to the CUMS paradigm shows decreased Ser-9 phosphorylation, increased Tyr-216 phosphorylation of GSK3 $\beta$ , and increased Ser-616 phosphorylation of the Kv4.2 subunit; 4) modulation of GSK3 $\beta$  (by pharmacological and shRNA means) reverses tLTP amplitude and Kv4.2-mediated currents in CUMS mice; and 5) GSK3 $\beta$  coimmunoprecipitates and colocalizes with the Kv4.2 subunit.

Changes in synaptic and structural plasticity induced by chronic stress exposure and depression have been well-characterized in the hippocampus. The chronic unpredictable stress model impairs LTP in CA1 and the dentate gyrus (DG) (63), while chronic restraint stress was found to impair LTP in CA3 (64). Another study demonstrated that CUMS impaired neurogenesis in the DG and facilitated LTD in CA1 (65). Consistent with loss of synaptic plasticity in the hippocampus, CUMS promotes pyramidal dendrite atrophy in CA1, CA2, and CA3 (66). Similarly, chronic immobilization stress promotes pyramidal dendrite retraction in CA1 and CA3 in an *N*-methyl-D-aspartate (NMDA) receptor-dependent manner (67). Similar changes in synaptic plasticity were reported in the prefrontal cortex following chronic stress (3, 68). However, other brain regions, such as the NAc and amygdala, which have received so far less attention, show an opposite regulation of neuroplasticity, with a gain in excitatory and loss of inhibitory synaptic tone in depression-like behavioral models (3). Along the same line, chronic social defeat stress causes an increase in spine density and miniature EPSP frequency in MSNs (69).

Our findings that CUMS enhances tLTP in MSNs provide supporting evidence for brain region-specific maladaptive plasticity associated with depression-like behavior. MSNs are typically classified as dopamine D1 receptor and dopamine D2 receptor subtypes, belonging to the direct pathway and indirect pathway,

respectively (70). Experimental evidence suggests that functional changes in the two MSN subpopulations mediate differential responses to stress (for a review, see ref. 4), and the role of each subtype in CUMS-induced changes of STDP remains to be elucidated.

In this study, we show that A-type  $K^+$  currents in MSNs are primarily mediated by the Kv4.2 channel subunit, whose activity is modulated by phosphorylation. Previous studies provided evidence for calcium/calmodulin-dependent kinase II (CaMKII) (71), PKA (72), and extracellular signal-regulated kinase (ERK) (73)-mediated phosphorylation of the Kv4.2 channel, the latter leading to decreased Kv4.2 current amplitude due to direct phosphorylation of the Ser-616 residue (74). Notably, Ser-616 lies in a putative GSK3 $\beta$  consensus motif. Recent evidence indicates that if phosphorylated by GSK3 $\beta$ , Ser-616 promotes decreased A-type  $K^+$  channel activity in layer 2/3 of the somatosensory cortex (38), confirming that Ser-616 is a converging site of multiple kinase signaling mechanisms.

In our current study, we showed that Ser-616 phosphorylation of Kv4.2 is critical for A-type  $K^+$  current modulation in MSNs and suggested that direct protein-protein interaction between the Kv4.2 subunit and GSK3 $\beta$  is likely responsible for this effect; of note, here we provide evidence for a functional role for this signaling mechanism in the context of depression-like behavior and maladaptive plasticity.

How does a GSK3 $\beta$ -dependent decrease of Kv4.2 channel activity lead to augmented tLTP in response to CUMS? It is well-known that A-type  $K^+$  channels contribute to synaptic plasticity regulation besides affecting action-potential repolarization (48). In particular, blocking A-type  $K^+$  currents with 4-aminopyridine enhances the backpropagation of dendritic APs and boosts EPSPs (75). Moreover, Kv4.2 gene deletion nearly abolishes A-type  $K^+$  currents, leading to increased intracellular  $Ca^{2+}$  levels in dendritic branches and a lower LTP induction threshold (48). Because  $Ca^{2+}$  influx is fundamental for many forms of synaptic plasticity in



dendrites, including STDP in the NAc (21), modulation of A-type  $K^+$  currents mediated by Kv4.2 channels is critical for synaptic processing during synaptic plasticity.

It is conceivable that Kv4.2 phosphorylation by GSK3 $\beta$  would trigger the aforementioned cascade of dendritic signaling events leading to the amplification of tLTP observed in CUMS animals. Opposite changes in tLTP would be consistent with down-regulation of GSK3 $\beta$  and subsequent increase of A-type  $K^+$  currents. GSK3 $\beta$  would then serve as a bidirectional switch that ultimately controls the magnitude of dendritic  $Ca^{2+}$  influx and consequently determines whether plasticity increases or decreases (20, 21, 76). It is noteworthy that our findings provide evidence for the involvement of ion channel-related mechanisms in the neurobiology of depression (29, 77).

Different studies have showed complex phosphorylation-dependent regulation of Kv4.2 with functional consequences for transient A-type  $K^+$  currents (78). In vitro phosphorylation of recombinant fragments of Kv4.2 revealed PKA (72), ERK (73), and CaMKII (71)-mediated phosphorylation of Kv4.2. It is noteworthy that ERK-mediated phosphorylation leads to decreased Kv4.2 and that ERK directly phosphorylates Kv4.2 at T602, T607, and Ser-616 (74). In particular, activation of ERK leads to a change in the voltage-dependent activation of Kv4.2 channels, causing a rightward shift in the activation curve and decreased rate of recovery from inactivation (79). With regard to PKA-mediated phosphorylation of Kv4.2, it has been shown that S552 is a prominent regulatory site in inducing activity-dependent internalization of Kv4.2 in neuronal dendrites (80, 81). Indeed, pharmacological activation of PKA leads to Kv4.2 internalization from dendritic spines, a process that is inhibited by the S552A mutation. PKA-mediated phosphorylation at S552 also enhanced surface expression of Kv4.2 induced by interaction with cytoplasmic  $K^+$  channel-interacting protein auxiliary subunits, an effect that requires phosphorylation at S552 (82). It remains to be addressed whether the CUMS protocol may affect Kv4.2 also through PKA and/or ERK.

The role of Kv4.2 channels in the GSK3 $\beta$  effects on tLTP is supported by strong evidence that the pharmacological blockade of A-type  $K^+$  currents by the selective Kv4 agent AmmTX3 mimics and occludes the CUMS effects on tLTP. Furthermore, pharmacological agents affecting GSK3 activity and GSK3 $\beta$  knockdown by in vivo genetic silencing lead to A-type  $K^+$  current modulation.

An increasing body of research has provided evidence for links between depression and increased GSK3 $\beta$  signaling. Enhanced GSK3 $\beta$  expression has been shown to correlate with nNOS expression in postmortem brains from MDD patients (83). In addition, decreased levels of inhibitory GSK3 $\beta$  phosphorylation at Ser-9 have been reported in the ventral prefrontal cortex of MDD patients, suggesting sustained GSK3 $\beta$  activity as a disease biomarker (84). Further support for a link between active GSK3 $\beta$  levels and depression-like behavior comes from animal studies. For example, the GSK3 $\beta^{+/+}$  knockin mouse model exhibits increased vulnerability to developing learned helplessness compared with wild-type mice (31), a phenotype that is ameliorated in heterozygous GSK3 $\beta^{+/-}$  mice (85).

Additionally, Nestler's group showed that GSK3 $\beta$  overexpression in the NAc recapitulates a depression-like phenotype (32) whereas a dominant-negative form of GSK3 $\beta$  overexpression in the NAc enhances resilience to subsequent stress in the social defeat paradigm. Interestingly, in accordance with the general notion of increased GSK3 $\beta$  signaling in depression, Wilkinson and colleagues (32) also showed a significant reduction in phosphorylation levels at Ser-9 of GSK3 $\beta$  in the NAc of social defeat mice that is in agreement with our findings in the NAc of CUMS-treated mice. Our data also demonstrate that GSK3 $\beta$  silencing in NAc shell MSNs sufficiently and effectively prevents depression-like behaviors in the CUMS mouse model of depression.

Previous studies using this AAV-shGSK3 $\beta$  in the NAc shell of rats found a prodepressant-like phenotype in nonstressed rats (37). However, it has been reported that other antidepressant manipulations, such as imipramine administration, exert opposite effects in the NAc of control vs. "depressed" rats (47).

In conclusion, we describe here a molecular mechanism underlying vulnerability to depression and related synaptic plasticity in the NAc. Our results indicate that the GSK3 $\beta$ -Kv4.2 complex plays a critical role in the MSN maladaptive plasticity occurring in the CUMS model that can be prevented by in vivo silencing of GSK3 $\beta$ . GSK3 $\beta$  knockdown also prevented CUMS-induced depressive-like behavior, thus suggesting that down-regulation of GSK3 $\beta$  activity may be a promising strategy to prevent maladaptive plasticity and behaviors in stress-induced psychiatric disorders. Our findings have a potential impact on novel, personalized medical therapeutic approaches for the treatment of MDD.

## Materials and Methods

A detailed description of the applied methods is given in *SI Appendix, Materials and Methods*. In the following, we give a brief account of our procedures.

**Animals and Ethical Approval.** Male C57BL/6J mice, bred in-house, were maintained on a 12-h light/dark cycle in a temperature- and humidity-controlled room with ad libitum access to mouse chow and water. Three to four-wk-old mice were used at the start of the experiments. All animal procedures were approved by the Ethics Committee of Università Cattolica del Sacro Cuore and complied with Italian Ministry of Health guidelines and with national laws (Legislative Decree 116/1992) and European Union guidelines on animal research (86/609/EEC).

**Chronic Unpredictable Mild Stress.** The stress procedure was modified from the chronic mild stress procedure described in previous studies (86). The CUMS paradigm consisted of daily exposure to alternating stressors along with occasional overnight stressors for 3 consecutive weeks. The stressors consisted of 1) 24 h of food and water deprivation, 2) 24 h in a wet and soiled cage, 3) 24 h in a horizontally tilted cage at 45°, 4) a 6-min cold swim at 10 °C, 5) overnight illumination, 6) a 2-min tail pinch, 7) 2 h of physical restraint, and 8) 18 h in a new cage without bedding. The different stressors (one for each day) were randomly distributed over 3 wk and the same stress sequence was not consistently applied to ensure the mice would be unable to anticipate the next type of stress that would be applied.

**Slice Preparation and Electrophysiology.** Coronal slices (300  $\mu$ m) containing the NAc were prepared as previously described (38). Recordings were performed using the MultiClamp 700B/Digidata 1550A System (Molecular Devices) digitized at a 10,000-Hz sampling frequency. All of the electrophysiological recordings were analyzed using Clampfit 10.9 software (Molecular Devices). Only cells with a stable resting membrane potential negative to  $-80$  mV, overshooting action potentials (exceeding 75 to 80 mV threshold to peak), and an input resistance  $>80$  M $\Omega$  were included. Furthermore, cells were rejected if resting membrane potential and input resistance changed more than 20%.

Excitatory postsynaptic potentials were recorded in whole-cell, current-clamp mode from NAc MSNs. Baseline EPSPs were recorded for 10 min at 0.2-Hz stimulation. To generate synaptic plasticity, we paired a single postsynaptic action potential elicited by brief somatic current injections (1 nA; 1 to 2 ms) and electrically driven EPSPs. In particular, a post-before-pre pairing protocol ( $\Delta t = -20$  ms) was applied 90 times at 1 Hz. Inhibitory inputs were not blocked using GABA $_A$  blockers. The change in EPSP slope was evaluated 35 to 40 min after the end of the pairing period and normalized to the baseline EPSP slope. The EPSP slope was measured as a linear fit between time points on the rising phase of the EPSP corresponding to 25 and 75% of the peak amplitude during control conditions. A more detailed description of the methodologies used in both current- and voltage-clamp recordings can be found in *SI Appendix*.

**Behavioral Assays.** All of the behavioral tests were performed in a soundproof room. The behavioral tests were monitored and recorded with a digital camera interfaced with a computer running ANY-maze video imaging software (Stoelting). After CUMS was completed, mice underwent multiple tests in the following order: elevated plus maze, forced swim test, and sucrose preference test, with at least a 24-h interval between tests.

**Elevated Plus Maze.** Anxiety responses were measured in the EPM test. The procedure was similar to the method of Lister (87). The apparatus consisted of two opposing open arms (30 × 5 cm) and two equal-sized closed (30 × 5 × 15 cm) arms opposite each other, made of Plexiglas and elevated at a height of 50 cm from the floor. Each mouse was placed in the central square (5 × 5 cm) facing an open arm and allowed to explore the maze for 5 min of the test period. The parameters measured were time spent in the open arm, time spent in the closed arm, and closed- and open-arm entrances. The maze was cleaned with dilute 70% alcohol before each session to get rid of residual odor.

**Forced Swim Test.** The forced swim test was administered as previously described (88). Mice were individually placed into a glass cylinder (20-cm diameter, 35-cm height) filled with water (23 ± 2 °C) to a height of 20 cm. Test sessions lasted 6 min and were video-recorded. The duration of behavioral immobility, reflecting behavioral despair, was measured manually by using ANY-maze analysis software (Stoelting). The amount of time spent immobile in the last 4 min of the test session was analyzed. A mouse was considered to be immobile when it stopped struggling and passively moved to remain floating and keep its head above water.

**Sucrose Preference Test.** Sucrose preference was performed as a measure of anhedonia. In the home cage, mice were habituated with two identical water bottles for 24 h. Water in one bottle was then replaced with 1.5% sucrose solution and mice were housed singly to perform the test. Bottle locations were randomly assigned and flipped at 12 h to prevent potential preference in side. The consumption of water and sucrose solution was measured 24 h later by weighing the bottles. Sucrose preference was calculated as a percentage of total intake:  $(\Delta\text{weight}_{\text{sucrose}})/(\Delta\text{weight}_{\text{sucrose}} + \Delta\text{weight}_{\text{water}}) \times 100\%$  (29).

**Virus Injection.** Adeno-associated viral vector (AAV2), which uses RNA interference to knock down GSK3 $\beta$  (AAV-shGSK3 $\beta$ ) and control vectors (AAV-shCTRL) used in this study, was previously constructed and validated (37). Viral injections were performed according to previous studies (29). Briefly, mice (3 to 4 wk of age) were anesthetized with a mix of ketamine (87.5 mg/kg) and xylazine (12.5 mg/kg). Viruses (0.8  $\mu$ L) were injected bilaterally into the

NAC shell (+1.8 mm anterior–posterior, ±0.9 mm medial–lateral, and –4.6 dorsal–ventral from bregma) with a 10-mL Hamilton syringe at a speed of 0.2  $\mu$ L/min. Experiments on mice injected with AAV2 were performed 1 wk after stereotaxic surgery to allow expression of viruses. In a subset of experiments, AAV-shGSK3 $\beta$  and AAV-shCTRL vectors were injected into mice that subsequently underwent CUMS protocols. All of the experiments involving virus injections were not performed at the same time of those carried out in control and CUMS mice.

**Western Blot Assay.** Tissues were lysed in ice-cold lysis buffer containing 1% Triton X-100, 0.1% sodium dodecyl sulfate (SDS), 1× protease inhibitor mixture (Sigma-Aldrich), 1 mM sodium orthovanadate (Sigma-Aldrich), and 1 mM sodium fluoride (Sigma-Aldrich). Lysates were incubated for 10 min on ice with occasional vortexing and spun down at 22,000 × g, 4 °C. Equal amounts of protein were diluted in Laemmli buffer, boiled, and resolved by SDS/PAGE. The primary antibodies (anti-Kv4.2 [OriGene], anti-Kv4.2/KCND2 phospho-Ser-616 [MyBioSource], anti-GSK3 $\beta$  [Cell Signaling], anti-GSK3 $\beta$  phospho-Ser-9 [Cell Signaling], anti-GFP [Thermo Fisher], and anti-tubulin [Sigma]) were incubated overnight and revealed with HRP-conjugated secondary antibodies (Cell Signaling). Expression was evaluated and documented by using Uvitec Cambridge Alliance.

**Statistical Analysis.** Data are expressed as means ± SEM. Statistical significance was assessed with either Student's *t* test or one-factor ANOVA for multiple-group comparisons (with Tukey post hoc test). Statistical analysis was performed with SYSTAT 10.2 software (Systat Software) and OriginPro 8.5 software (OriginLab). Each series of data was analyzed with the ROUT method (*Q* = 1%) for detecting outliers that were not included in statistical analyses and graphs. The level of significance was set at 0.05.

**Data Availability.** The datasets generated and/or analyzed during the current study are available from the corresponding author on reasonable request.

**ACKNOWLEDGMENTS.** This work was supported by intramural grants from Università Cattolica del Sacro Cuore (to C.G.) and NIH Grants R01MH111107 (to F.L.), R01MH095995 (to F.L.), and R01DA047102 (to T.A.G. and F.L.).

- Otte C, et al. Major depressive disorder. *Nat. Rev. Dis. Primers* 2, 16065 (2016).
- Ferrari A, et al. Global variation in the prevalence and incidence of major depressive disorder: A systematic review of the epidemiological literature. *Psychol. Med.* 43, 471–481 (2013).
- Marsden W, et al. Synaptic plasticity in depression: Molecular, cellular and functional correlates. *Prog. Neuropsychopharmacol. Biol. Psychiatry* 43, 168–184 (2013).
- Francis T, et al. Emerging role for nucleus accumbens medium spiny neuron subtypes in depression. *Biol. Psychiatry* 81, 645–653 (2017).
- Ali A, et al. Glycogen synthase kinase-3: Properties, functions, and regulation. *Chem. Rev.* 101, 2527–2540 (2001).
- Takahashi M, et al. Localization and developmental changes of tau protein kinase II/glycogen synthase kinase-3 beta in rat brain. *J. Neurochem.* 63, 245–255 (1994).
- Wei J, et al. Regulation of AMPA receptor trafficking and function by glycogen synthase kinase 3. *J. Biol. Chem.* 285, 26369–26376 (2010).
- Bradley C, et al. A pivotal role of GSK-3 in synaptic plasticity. *Front. Mol. Neurosci.* 5, 13 (2012).
- Jope R, et al. The glamour and gloom of glycogen synthase kinase-3. *Trends Biochem. Sci.* 29, 95–102 (2004).
- Hur E, et al. GSK3 signalling in neural development. *Nat. Rev. Neurosci.* 11, 539–551 (2010).
- Beurel R, et al. The paradoxical pro- and anti-apoptotic actions of GSK3 in the intrinsic and extrinsic apoptosis signaling pathways. *Prog. Neurobiol.* 79, 173–189 (2006).
- Tamura M, et al. Developmental inhibition of Gsk3 rescues behavioral and neurophysiological deficits in a mouse model of schizophrenia predisposition. *Neuron* 89, 1100–1109 (2016).
- Kremer A, et al. Facts and fiction. *Front. Mol. Neurosci.* 4, 17 (2011).
- Miller J, et al. Cocaine-induced hyperactivity and sensitization are dependent on GSK3. *Neuropharmacology* 56, 1116–1123 (2009).
- Jope R, et al. Glycogen synthase kinase-3 in the etiology and treatment of mood disorders. *Front. Mol. Neurosci.* 4, 16 (2011).
- Kockeritz L, et al. Glycogen synthase kinase-3—An overview of an over-achieving protein kinase. *Curr. Drug Targets* 7, 1377–1388 (2006).
- Peineau S, et al. A systematic investigation of the protein kinases involved in NMDA receptor-dependent LTD: Evidence for a role of GSK-3 but not other serine/threonine kinases. *Mol. Brain* 2, 22 (2009).
- Willner P. The chronic mild stress (CMS) model of depression: History, evaluation and usage. *Neurobiol. Stress* 6, 78–93 (2016).
- Brzosko Z, et al. Neuromodulation of spike-timing-dependent plasticity: Past, present, and future. *Neuron* 103, 563–581 (2019).
- Feldman D. The spike-timing dependence of plasticity. *Neuron* 75, 556–571 (2012).
- Ji X, et al. New rules governing synaptic plasticity in core nucleus accumbens medium spiny neurons. *Eur. J. Neurosci.* 36, 3615–3627 (2012).
- Krause M, et al. A pause in nucleus accumbens neuron firing is required to initiate and maintain feeding. *J. Neurosci.* 30, 4746–4756 (2010).
- Puig M, et al. In vivo modulation of the activity of pyramidal neurons in the rat medial prefrontal cortex by 5-HT2A receptors: Relationship to thalamocortical afferents. *Cereb. Cortex* 13, 870–882 (2003).
- Rosenkranz J, et al. Modulation of basolateral amygdala neuronal firing and afferent drive by dopamine receptor activation in vivo. *J. Neurosci.* 19, 11027–11039 (1999).
- Hopf F, et al. Cooperative activation of dopamine D1 and D2 receptors increases spike firing of nucleus accumbens neurons via G-protein betagamma subunits. *J. Neurosci.* 23, 5079–5087 (2003).
- Scala F, et al. Environmental enrichment and social isolation mediate neuroplasticity of medium spiny neurons through the GSK3 pathway. *Cell Rep.* 23, 555–567 (2018).
- Xi X, et al. Dopamine receptors differentially control binge alcohol drinking-mediated synaptic plasticity of the core nucleus accumbens direct and indirect pathways. *J. Neurosci.* 37, 5463–5474 (2017).
- Chatterjee M, et al. Evaluation of the antipsychotic potential of *Panax quinquefolium* in ketamine induced experimental psychosis model in mice. *Neurochem. Res.* 37, 759–770 (2012).
- Cheng J, et al. Greenard, HCN2 channels in cholinergic interneurons of nucleus accumbens shell regulate depressive behaviors. *Neuron* 101, 662–672.e5 (2019).
- Hogg S. A review of the validity and variability of the elevated plus-maze as an animal model of anxiety. *Pharmacol. Biochem. Behav.* 54, 21–30 (1996).
- Polter A, et al. Deficiency in the inhibitory serine-phosphorylation of glycogen synthase kinase-3 increases sensitivity to mood disturbances. *Neuropsychopharmacology* 35, 1761–1774 (2010).
- Wilkinson M, et al. A novel role of the WNT-dishevelled-GSK3 $\beta$  signaling cascade in the mouse nucleus accumbens in a social defeat model of depression. *J. Neurosci.* 31, 9084–9092 (2011).
- Hughes K, et al. Modulation of the glycogen synthase kinase-3 family by tyrosine phosphorylation. *EMBO J.* 12, 803–808 (1993).
- Doble B, et al. Tricks of the trade for a multi-tasking kinase. *J. Cell Sci.* 116, 1175–1186 (2003).
- Rayasam G, et al. Glycogen synthase kinase 3: More than a namesake. *Br. J. Pharmacol.* 156, 885–898 (2009).
- Choi H, et al. Rapid detection of glycogen synthase kinase-3 activity in mouse sperm using fluorescent gel shift electrophoresis. *Sensors (Basel)* 16, 551 (2016).

37. E. J. Crofton *et al.*, Glycogen synthase kinase 3 beta alters anxiety-, depression-, and addiction-related behaviors and neuronal activity in the nucleus accumbens shell. *Neuropharmacology* **117**, 49–60 (2017).
38. G. Aceto *et al.*, GSK3 $\beta$  modulates timing-dependent long-term depression through direct phosphorylation of Kv4.2 channels. *Cereb. Cortex* **29**, 1851–1865 (2019).
39. C. R. Cadwell *et al.*, Multimodal profiling of single-cell morphology, electrophysiology, and gene expression using patch-seq. *Nat. Protoc.* **12**, 2531–2553 (2017).
40. J. Fuzik *et al.*, Integration of electrophysiological recordings with single-cell RNA-seq data identifies neuronal subtypes. *Nat. Biotechnol.* **34**, 175–183 (2016).
41. J. Jo *et al.*, A $\beta$ (1–42) inhibition of LTP is mediated by a signaling pathway involving caspase-3, Akt1 and GSK-3 $\beta$ . *Nat. Neurosci.* **14**, 545–547 (2011).
42. A. V. Franklin *et al.*, Glycogen synthase kinase-3 inhibitors reverse deficits in long-term potentiation and cognition in fragile X mice. *Biol. Psychiatry* **75**, 198–206 (2014).
43. R. J. Chen *et al.*, Variations in glycogen synthesis in human pluripotent stem cells with altered pluripotent states. *PLoS One* **10**, e0142554 (2015).
44. W. C. Hsu *et al.*, Identifying a kinase network regulating FGF14:Nav1.6 complex assembly using split-luciferase complementation. *PLoS One* **10**, e0117246 (2015).
45. S. Kailanathan *et al.*, Activation of a synapse weakening pathway by human Val66 but not Met66 pro-brain-derived neurotrophic factor (proBDNF). *Pharmacol. Res.* **104**, 97–107 (2016).
46. E. S. Emamian, D. Hall, M. J. Birnbaum, M. Karayiorgou, J. A. Gogos, Convergent evidence for impaired AKT1-GSK3 $\beta$  signaling in schizophrenia. *Nat. Genet.* **36**, 131–137 (2004).
47. D. L. Wallace *et al.*, CREB regulation of nucleus accumbens excitability mediates social isolation-induced behavioral deficits. *Nat. Neurosci.* **12**, 200–209 (2009).
48. X. Chen *et al.*, Deletion of Kv4.2 gene eliminates dendritic A-type K<sup>+</sup> current and enhances induction of long-term potentiation in hippocampal CA1 pyramidal neurons. *J. Neurosci.* **26**, 12143–12151 (2006).
49. A. J. Norris, J. M. Nerbonne, Molecular dissection of I(A) in cortical pyramidal neurons reveals three distinct components encoded by Kv4.2, Kv4.3, and Kv1.4 alpha-subunits. *J. Neurosci.* **30**, 5092–5101 (2010).
50. J. K. Maffie, E. Dvoretzka, P. E. Bougis, M. F. Martin-Eauclaire, B. Rudy, Dipeptidyl-peptidase-like-proteins confer high sensitivity to the scorpion toxin AamTX3 to Kv4-mediated A-type K<sup>+</sup> channels. *J. Physiol.* **591**, 2419–2427 (2013).
51. Q. Li *et al.*, Long-term modulation of A-type K(+) conductances in hippocampal CA1 interneurons in rats after chronic intermittent ethanol exposure during adolescence or adulthood. *Alcohol. Clin. Exp. Res.* **37**, 2074–2085 (2013).
52. F. Scala *et al.*, Intraneuronal A $\beta$  accumulation induces hippocampal neuron hyperexcitability through A-type K(+) current inhibition mediated by activation of caspases and GSK-3. *Neurobiol. Aging* **36**, 886–900 (2015).
53. W. A. Coetzee *et al.*, Molecular diversity of K<sup>+</sup> channels. *Ann. N. Y. Acad. Sci.* **868**, 233–285 (1999).
54. A. D. Wickenden, R. G. Tsushima, V. A. Losito, R. Kaprielian, P. H. Backx, Effect of Cd<sup>2+</sup> on Kv4.2 and Kv1.4 expressed in *Xenopus* oocytes and on the transient outward currents in rat and rabbit ventricular myocytes. *Cell. Physiol. Biochem.* **9**, 11–28 (1999).
55. S. G. Birnbaum *et al.*, Structure and function of Kv4-family transient potassium channels. *Physiol. Rev.* **84**, 803–833 (2004).
56. P. R. Mendonça *et al.*, Stochastic and deterministic dynamics of intrinsically irregular firing in cortical inhibitory interneurons. *eLife* **5**, e16475 (2016).
57. D. Pathak, D. Guan, R. C. Foehring, Roles of specific Kv channel types in repolarization of the action potential in genetically identified subclasses of pyramidal neurons in mouse neocortex. *J. Neurophysiol.* **115**, 2317–2329 (2016).
58. C. M. McDermott, L. A. Schrader, Activation of  $\kappa$  opioid receptors increases intrinsic excitability of dentate gyrus granule cells. *J. Physiol.* **589**, 3517–3532 (2011).
59. J. Kim, D. S. Wei, D. A. Hoffman, Kv4 potassium channel subunits control action potential repolarization and frequency-dependent broadening in rat hippocampal CA1 pyramidal neurons. *J. Physiol.* **569**, 41–57 (2005).
60. H. Akil *et al.*, Treatment resistant depression: A multi-scale, systems biology approach. *Neurosci. Biobehav. Rev.* **84**, 272–288 (2018).
61. S. Antoniuk, M. Bijata, E. Ponimaskin, J. Wlodarczyk, Chronic unpredictable mild stress for modeling depression in rodents: Meta-analysis of model reliability. *Neurosci. Biobehav. Rev.* **99**, 101–116 (2019).
62. M. N. Hill, K. G. Hellemans, P. Verma, B. B. Gorzalka, J. Weinberg, Neurobiology of chronic mild stress: Parallels to major depression. *Neurosci. Biobehav. Rev.* **36**, 2085–2117 (2012).
63. D. N. Alfarez, M. Joëls, H. J. Krugers, Chronic unpredictable stress impairs long-term potentiation in rat hippocampal CA1 area and dentate gyrus in vitro. *Eur. J. Neurosci.* **17**, 1928–1934 (2003).
64. C. Pavlides, L. G. Nivón, B. S. McEwen, Effects of chronic stress on hippocampal long-term potentiation. *Hippocampus* **12**, 245–257 (2002).
65. R. Holderbach, K. Clark, J. L. Moreau, J. Bischofberger, C. Normann, Enhanced long-term synaptic depression in an animal model of depression. *Biol. Psychiatry* **62**, 92–100 (2007).
66. L. Luo, R. X. Tan, Fluoxetine inhibits dendrite atrophy of hippocampal neurons by decreasing nitric oxide synthase expression in rat depression model. *Acta Pharmacol. Sin.* **22**, 865–870 (2001).
67. K. M. Christian, A. D. Miracle, C. L. Wellman, K. Nakazawa, Chronic stress-induced hippocampal dendritic retraction requires CA3 NMDA receptors. *Neuroscience* **174**, 26–36 (2011).
68. M. Quan *et al.*, Impairments of behavior, information flow between thalamus and cortex, and prefrontal cortical synaptic plasticity in an animal model of depression. *Brain Res. Bull.* **85**, 109–116 (2011).
69. D. J. Christoffel *et al.*, I $\kappa$ B kinase regulates social defeat stress-induced synaptic and behavioral plasticity. *J. Neurosci.* **31**, 314–321 (2011).
70. Y. M. Kupchik *et al.*, Coding the direct/indirect pathways by D1 and D2 receptors is not valid for accumbens projections. *Nat. Neurosci.* **18**, 1230–1232 (2015).
71. A. W. Varga *et al.*, Calcium-calmodulin-dependent kinase II modulates Kv4.2 channel expression and upregulates neuronal A-type potassium currents. *J. Neurosci.* **24**, 3643–3654 (2004).
72. A. E. Anderson *et al.*, Kv4.2 phosphorylation by cyclic AMP-dependent protein kinase. *J. Biol. Chem.* **275**, 5337–5346 (2000).
73. J. P. Adams *et al.*, The A-type potassium channel Kv4.2 is a substrate for the mitogen-activated protein kinase ERK. *J. Neurochem.* **75**, 2277–2287 (2000).
74. L. A. Schrader *et al.*, ERK/MAPK regulates the Kv4.2 potassium channel by direct phosphorylation of the pore-forming subunit. *Am. J. Physiol. Cell Physiol.* **290**, C852–C861 (2006).
75. D. A. Hoffman, J. C. Magee, C. M. Colbert, D. Johnston, K<sup>+</sup> channel regulation of signal propagation in dendrites of hippocampal pyramidal neurons. *Nature* **387**, 869–875 (1997).
76. T. Nevia, B. Sakmann, Spine Ca<sup>2+</sup> signaling in spike-timing-dependent plasticity. *J. Neurosci.* **26**, 11001–11013 (2006).
77. Y. Cui *et al.*, Astroglial Kir4.1 in the lateral habenula drives neuronal bursts in depression. *Nature* **554**, 323–327 (2018).
78. O. Cerda, J. S. Trimmer, Analysis and functional implications of phosphorylation of neuronal voltage-gated potassium channels. *Neurosci. Lett.* **486**, 60–67 (2010).
79. L. L. Yuan, J. P. Adams, M. Swank, J. D. Sweatt, D. Johnston, Protein kinase modulation of dendritic K<sup>+</sup> channels in hippocampus involves a mitogen-activated protein kinase pathway. *J. Neurosci.* **22**, 4860–4868 (2002).
80. J. Kim, S. C. Jung, A. M. Clemens, R. S. Petralia, D. A. Hoffman, Regulation of dendritic excitability by activity-dependent trafficking of the A-type K<sup>+</sup> channel subunit Kv4.2 in hippocampal neurons. *Neuron* **54**, 933–947 (2007).
81. R. S. Hammond, L. Lin, M. S. Sidorov, A. M. Wikenheiser, D. A. Hoffman, Protein kinase A mediates activity-dependent Kv4.2 channel trafficking. *J. Neurosci.* **28**, 7513–7519 (2008).
82. L. Lin, W. Sun, A. M. Wikenheiser, F. Kung, D. A. Hoffman, KChIP4a regulates Kv4.2 channel trafficking through PKA phosphorylation. *Mol. Cell. Neurosci.* **43**, 315–325 (2010).
83. D. H. Oh, Y. C. Park, S. H. Kim, Increased glycogen synthase kinase-3 $\beta$  mRNA level in the hippocampus of patients with major depression: A study using the Stanley Neuropathology Consortium Integrative Database. *Psychiatry Investig.* **7**, 202–207 (2010).
84. F. Karege *et al.*, Alteration in kinase activity but not in protein levels of protein kinase B and glycogen synthase kinase-3 $\beta$  in ventral prefrontal cortex of depressed suicide victims. *Biol. Psychiatry* **61**, 240–245 (2007).
85. W. T. O'Brien *et al.*, Glycogen synthase kinase-3 $\beta$  haploinsufficiency mimics the behavioral and molecular effects of lithium. *J. Neurosci.* **24**, 6791–6798 (2004).
86. P. Willner, Validity, reliability and utility of the chronic mild stress model of depression: A 10-year review and evaluation. *Psychopharmacology (Berl.)* **134**, 319–329 (1997).
87. R. G. Lister, The use of a plus-maze to measure anxiety in the mouse. *Psychopharmacology (Berl.)* **92**, 180–185 (1987).
88. A. Mastrodonato *et al.*, Ventral CA3 activation mediates prophylactic ketamine efficacy against stress-induced depressive-like behavior. *Biol. Psychiatry* **84**, 846–856 (2018).